

Wide-Range Robust Control of Combustion Instability

BOE-SHONG HONG, ASOK RAY, and VIGOR YANG*

Department of Mechanical Engineering, The Pennsylvania State University, University Park, PA 16802, USA

This paper presents the concept and design of a two-layer robust control system for suppression of combustion instabilities over a wide range of operation. The control law is synthesized based on a multiple-time-scale model of combustion dynamics. Control actions on the fast-time scale are provided by secondary fuel injection, and are gain-scheduled according to the variations of mean-flow temperature and velocity on the slow-time scale. A linear parameter varying (LPV) L_2 -gain control law is formulated in the setting of differential game theory. Simulation experiments have been conducted to evaluate the control law under wide-range operation of a generic combustor in terms of the trade-off among: (1) fuel injection rate and pressure oscillation; (2) transient and steady responses; and (3) stability robustness and performance. © 2002 by The Combustion Institute

NOMENCLATURE FOR MODEL FORMULATION PART

\bar{a}	Speed of sound in mixture
b_k	Spatial distribution of burning of control fuel at k th location
\bar{C}_v	Constant-volume specific heat for two-phase mixture
D_{ni}	Linear parameters, Eq. 35
E_{ni}	Linear parameters, Eq. 35
ΔH_c	Heat of combustion of control fuel
h	Source term in wave equation
L	Length of combustion chamber
\dot{m}_m	Mass flow rate of control fuel
p	Pressure
\bar{R}	Gas constant for two-phase mixture
\mathbf{r}	Position vector
T	Temperature
t	Time
t_f	Fast time
t_s	Slow time
V	Volume of combustion chamber
U_n	Control input of n th mode
\mathbf{v}_g	Velocity of gas phase
z	Axial coordinate

Greek Symbols

ρ	Density of two-phase mixture
ϑ	Gain-scheduling vector
ψ_n	Normal mode function of n th mode
ϕ	Space function of mean-flow quantities
η	Amplitudes of mode shapes
η_n	Time-varying amplitude of n th mode
$\bar{\gamma}$	Specific heat ratio for mixture

* Corresponding author. E-mail: vigor@psu.edu

ω_n	Normal frequency of n th mode
τ_k	Time delay of k th combustion control source
τ_v	Viscous stress tensor

Superscripts

\sim	Mean quantity
'	Perturbed quantity
\wedge	Laplace transform

Subscripts

c	Control input
g	Gas phase
l	Liquid phase
t	Gain-scheduling variable

NOMENCLATURE FOR CONTROLLER DESIGN PART

A_p	System parameter of nominal plant
A	Actuator dynamics
C_2	Nominal plant parameter associated with measurement
d	Plant disturbance
D	Right compensated function of generalized plant
D^{-1}	Left compensated function of generalized plant
G_1	Nominal plant parameter associated with control action
G_2	Nominal plant parameter associated with plant disturbance
K	Dynamics of LPV robust controller
\dot{m}_m	Mass flow rate of secondary fuel

q	Weighting factor associated with pressure response
P	Dynamics of gain-scheduled generalized plant
s	Laplace transform variable
u	Control signal of secondary-fuel injection
v	Control outputs of distributed actuators
x_p	State vector of nominal plant
y	Output vector of measurement
w_s	Disturbances induced from plant uncertainties
w_τ	Disturbances induced from time-delay errors
w_d	Weighted plant disturbance
w_θ	Weighted sensor noise
w	Generic disturbance
W_d	Shaping filter associated with plant disturbance
W_θ	Shaping filter associated with sensor noise
W_p	Performance weighting function associated with pressure response
W_u	Performance weighting function associated with control-fuel injection
W_τ	Stability weighting function associated time delay errors
z_s	Stability variable associated with plant uncertainty
z_p	Performance variable associated with pressure response
z_u	Performance variable associated with secondary-fuel injection
z_τ	Stability variable associated with time delay errors
z	Objective variable

Greek Symbols

Δ_p	Dynamics of normalized plant uncertainty
Δ_τ	Dynamics of phase uncertainty induced by time delay errors
δ_p	Plant uncertainty bound
ϑ	Gain-scheduling vector
η	Amplitudes of modes shapes
θ	Sensor noise

INTRODUCTION

Unsteady motions in confined combustion chambers often result from mean-flow depen-

dent interactions between heat release and acoustic oscillations. The underlying physical mechanisms involve a wide range of time scales that can be broadly classified into two categories: one representing mean-flow variations on a slow-time scale and the other representing acoustic oscillations on a fast-time scale. The disparity of time scales allows for the development of a hierarchically structured control law for regulating the various processes involved. The entire control system consists of two interacting modules: a slow-time supervisory controller and a fast-time flame controller, as illustrated in Fig. 1 [1]. The slow-time supervisory controller in the outer loop attempts to optimize the overall combustor performance and pollutant emissions based on the measurements of quasi-steady variables, and to identify the flame control parameters that determine the operating points of the fast dynamic phenomena such as pressure oscillations. The flame controller in the inner loop is responsible for suppression of combustion instability and for prevention of lean blowout of the flame. When coupled with a global engine control system, such a two-layer strategy will lead to an energy-efficient and clean system for propulsion and power-generation applications.

As part of their research on feedback control of combustion instabilities in various propulsion systems, Yang and co-workers established a series of robust control laws with distributed actuation [2–6]. The recent work by Hong et al. [5] was based on the H_∞ -optimization, which guaranteed robust stability and performance within specified bounds of model and parameter uncertainties as well as sensor noises and plant disturbances. The system parameters, however, were treated as time-invariant constants, thereby rendering the control laws valid only for fixed operating conditions. The present paper attempts to remedy this deficiency by taking into account the temporal variation of mean-flow dynamics in a unified manner, such that the resultant control laws function effectively over a wide range of operation. The work incorporates an H_∞ -based linear-parameter-varying (LPV) control law [7, 8] for modulating combustion dynamics. Its major contributions are summarized below.

1. Development of the concept of a multiple-time scale, multiple-layer control system for wide-range control of combustion instabilities; and
2. Formulation of an observer-embedded LPV control law for robust state estimation and control which, unlike the control law of Wu et al. [7], does not require on-line measurements of parameter variation rates.

The paper is organized in six sections including the introduction. The second section develops a two-time-scale model of combustion dynamics, which decomposes the overall combustor behavior into quasi-steady system performance in the slow-time scale and combustion oscillations in the fast-time scale. The LPV robust control law for wide-range operation is then formulated and analyzed in the third and fourth sections, respectively, based on the concept of differential game theory. The fifth section presents the results of simulation experiments and a comparison of the system responses under different control laws. The paper is summarized and concluded in the last section with recommendations for future research.

A TWO-TIME-SCALE MODEL OF COMBUSTION DYNAMICS

In this section, a series of theoretical modeling tools are applied to develop a two-time-scale model of combustion dynamics. The objective is to formulate a general framework for active control of combustion instabilities in liquid-fueled propulsion systems. The equations governing the combustion-fluid dynamics with feedback control inputs of mass, momentum, and energy are succinctly expressed as [2]:

$$\frac{\partial \rho}{\partial t} + \mathbf{v}_g \cdot \nabla \rho = W + W_c \quad (1)$$

$$\rho \frac{\partial \mathbf{v}_g}{\partial t} + \rho \mathbf{v}_g \cdot \nabla \mathbf{v}_g + \nabla p = \mathbf{F} + \mathbf{F}_c \quad (2)$$

$$\frac{\partial p}{\partial t} + \bar{\gamma} p \nabla \cdot \mathbf{v}_g + \mathbf{v}_g \cdot \nabla p = P + P_c \quad (3)$$

where the source terms W , \mathbf{F} , and P represent two-phase interactions and combustion influence, and W_c , \mathbf{F}_c and P_c the corresponding control inputs.

Both experimental and computational obser-

TABLE 1
Two Time-Scaled Motions

	Time Scales	Amplitude Orders
Mean-flow motion $\bar{x}(t_s)$	$t_s = \epsilon_s t$	$A_s \approx \epsilon_s A_t$
Acoustic motion $x'(t_f)$	$t_f = \epsilon_f t$	$A_f \approx \epsilon_f A_t$

vations show that the combustion chamber dynamics take place in two time scales: one representing mean-flow motions with a slow time scale and large amplitude order; and the other representing acoustic motions with a fast time scale and small amplitude order. Each of the conservation Eqs. 1 through 3 can thus be decomposed into two time scales, describing the slow behavior of mean flowfield and main-fuel injection, and the fast behavior of acoustic oscillations and secondary-fuel injection into the combustion chamber. By using a spatial averaging procedure equivalent to modal analysis, a linear finite-dimensional parameterized model can be derived for synthesis of a linear parameter varying (LPV) robust feedback control law.

Table 1 lists the time scales and amplitude orders of the fluid variables, ρ , \mathbf{v}_g , and p , where the subscripts s and f represent the slow and fast motions, respectively. The reference time t and amplitude order A_t are described in the slow and fast time scales by a pair of dimensionless parameters (ϵ_s , ϵ_f) with $\epsilon_f \sim o^1(\epsilon_s)$ where $|o^1(\theta)/\theta| \rightarrow 0$ as $\theta \rightarrow 0$. Note that t is the regular time used in the physical laws of Eqs. 1 through 3.

Remark 1

When observing events in the fast-time scale, $t_f \sim t$ implying that $\epsilon_f \sim 1$ and $\epsilon_s \gg 1$. Similarly, when observing events in the slow-time scale, $t_s \sim t$ implying that $\epsilon_s \sim 1$ and $\epsilon_f \ll 1$.

The combustion control inputs (W_c , \mathbf{F}_c , P_c) are also decomposed as two components. The primary component represents the mean-flow motions in the slow time scale and high amplitude order. The secondary component represents acoustic oscillations in the fast time scale and small amplitude order. Similar treatments are applied to the source terms (W , \mathbf{F} , P) due to uncontrolled combustion processes.

The universally independent variable in the time domain is the regular time t . However, for separation of the local and global behavior, the

flow variables $\mathbf{x} \equiv [\rho \ p \ \mathbf{v}_g]^\top$ are treated in the form $\mathbf{x}(\mathbf{r}, t) \equiv \mathbf{x}[\mathbf{r}, t_f(t), t_s(t)]$ which, in turn, is decomposed into the fast and slow components by perturbation analysis such that:

$$\mathbf{x}(\mathbf{r}, t_f, t_s) \equiv \bar{\mathbf{x}}(\mathbf{r}, t_s) + \mathbf{x}'(\mathbf{r}, t_f, t_s) \quad (4)$$

where the perturbation part \mathbf{x}' is governed by acoustic motions in the fast time t_f , and the average part $\bar{\mathbf{x}}$ represents the mean-flow motions in the slow time t_s . Formulation of a two-time-scale model following the structure in Eq. 4 is presented below.

When observing an event, the (local) time-derivative terms in Eqs. 1 through 3 are decomposed in the fast and slow time scales. For example, the gas velocity in the combustion chamber is decomposed as:

$$\begin{aligned} \frac{\partial \mathbf{v}_g[\mathbf{r}, t_f(t), t_s(t)]}{\partial t} &= \frac{\partial \mathbf{v}_g}{\partial t_s} \frac{dt_s}{dt} + \frac{\partial \mathbf{v}_g}{\partial t_f} \frac{dt_f}{dt} \\ &\equiv \frac{\partial \tilde{\mathbf{v}}_g}{\partial t_s} \epsilon_s + \frac{\partial \mathbf{v}'_g}{\partial t_f} \epsilon_f \end{aligned}$$

Equation 5 implies that the fluid variables ρ , \mathbf{v}_g and p can be linearly expanded as:

$$\left. \begin{aligned} \rho(\mathbf{r}, t) &\equiv \bar{\rho}(\mathbf{r}, t_s) + \rho'(\mathbf{r}, t_s, t_f) \\ \mathbf{v}_g(\mathbf{r}, t) &\equiv \tilde{\mathbf{v}}_g(\mathbf{r}, t_s) + \mathbf{v}'_g(\mathbf{r}, t_s, t_f) \\ p(\mathbf{r}, t) &\equiv \bar{p}(\mathbf{r}, t_s) + p'(\mathbf{r}, t_s, t_f) \end{aligned} \right\} \quad (4)$$

While the slow-time variables characterize system performance, the fast-time variables are related to the internal stability of the control system. The terms $\mathbf{v}_g \cdot \nabla \rho$; $\rho \mathbf{v}_g \cdot \nabla \mathbf{v}_g + \nabla p$; $\bar{\gamma} p \nabla \cdot \mathbf{v}_g + \mathbf{v}_g \cdot \nabla p$; (W , F , P); and (W_c , F_c , P_c) in Eqs. 1 through 3 are decomposed into two parts by Taylor series expansion in the slow time scale, based on Eq. 6 and the magnitude orders in Table 1. For example,

$$\begin{aligned} f[\mathbf{x}(t_f, t_s)] &= f[\bar{\mathbf{x}}(t_s)] + \left. \frac{\partial f}{\partial \mathbf{x}} \right|_{\bar{\mathbf{x}}(t_s)} \mathbf{x}'(t_f) \\ &\quad + \text{higher order terms} \end{aligned} \quad (7)$$

The term $\mathbf{v}_g \cdot \nabla \rho$ in Eq. 1 is decomposed as:

$$\begin{aligned} \mathbf{v}_g \cdot \nabla \rho &\equiv \tilde{\mathbf{v}}_g \cdot \nabla \bar{\rho}(\mathbf{r}, t_s) + \tilde{\mathbf{v}}_g(\mathbf{r}, t_s) \cdot \nabla \rho'(\mathbf{r}, t_s, t_f) \\ &\quad + \mathbf{v}'_g(\mathbf{r}, t_s, t_f) \cdot \nabla \bar{\rho}(\mathbf{r}, t_s) \end{aligned} \quad (8)$$

Similarly, the term $\rho \partial \mathbf{v}_g / \partial t$ in Eq. 2 is decomposed as:

$$\rho \frac{\partial \mathbf{v}_g}{\partial t} \equiv (\bar{\rho} + \rho') \left(\frac{\partial \tilde{\mathbf{v}}_g}{\partial t_s} \epsilon_s + \frac{\partial \mathbf{v}'_g}{\partial t_f} \epsilon_f \right) \quad (9)$$

which can be further approximated to first-order accuracy as:

$$\rho \frac{\partial \mathbf{v}_g}{\partial t} \approx \epsilon_s \bar{\rho} \frac{\partial \tilde{\mathbf{v}}_g}{\partial t_s} + \epsilon_s \rho' \frac{\partial \tilde{\mathbf{v}}_g}{\partial t_s} + \epsilon_f \bar{\rho} \frac{\partial \mathbf{v}'_g}{\partial t_f} \quad (10)$$

By using the above first-order approximations in Eqs. 5, 7, and 10, the conservation equations, 1 through 3, are decomposed in two time scales as follows.

Slow-Time Conservation Laws:

$$\text{Mass:} \quad \epsilon_s \frac{\partial \bar{\rho}}{\partial t_s} + \tilde{\mathbf{v}}_g \cdot \nabla \bar{\rho} = \bar{W} + \bar{W}_c \quad (11)$$

$$\text{Momentum:} \quad \epsilon_s \bar{\rho} \frac{\partial \tilde{\mathbf{v}}_g}{\partial t_s} + \bar{\rho} \tilde{\mathbf{v}}_g \cdot \nabla \tilde{\mathbf{v}}_g + \nabla \bar{p} = \bar{F} + \bar{F}_c \quad (12)$$

$$\begin{aligned} \text{Energy:} \quad \epsilon_s \frac{\partial \bar{p}}{\partial t_s} + \bar{\gamma} \bar{p} \nabla \cdot \tilde{\mathbf{v}}_g + \tilde{\mathbf{v}}_g \cdot \nabla \bar{p} \\ = \bar{P} + \bar{P}_c \end{aligned} \quad (13)$$

Fast-time Conservation Laws:

Mass:

$$\epsilon_f \frac{\partial \rho'}{\partial t_f} + \tilde{\mathbf{v}}_g \cdot \nabla \rho' + \mathbf{v}'_g \cdot \nabla \bar{\rho} = W' + W'_c \quad (14)$$

Momentum

$$\begin{aligned} \epsilon_f \bar{\rho} \frac{\partial \mathbf{v}'_g}{\partial t_f} + \nabla p' = -\bar{\rho} [\tilde{\mathbf{v}}_g \cdot \nabla \mathbf{v}'_g + \mathbf{v}'_g \cdot \nabla \tilde{\mathbf{v}}_g] \\ - \rho' \left(\epsilon_s \frac{\partial \tilde{\mathbf{v}}_g}{\partial t_s} + \tilde{\mathbf{v}}_g \cdot \nabla \tilde{\mathbf{v}}_g \right) + F' + F'_c \end{aligned} \quad (15)$$

Energy

$$\begin{aligned} \epsilon_f \frac{\partial p'}{\partial t_f} + \bar{\gamma} \bar{p} \nabla \cdot \mathbf{v}'_g = -\bar{\gamma} p' \nabla \cdot \tilde{\mathbf{v}}_g - \tilde{\mathbf{v}}_g \cdot \nabla p' \\ - \mathbf{v}'_g \cdot \nabla \bar{p} + P' + P'_c \end{aligned}$$

Combining the fast-time derivative of the energy Eq. 16 with the spatial derivative of the momentum Eq. 15 yields a wave equation governing the acoustic motions in the chamber.

$$\begin{aligned} \nabla^2 p'(\mathbf{r}, t_s, t_f) - \frac{\epsilon_f^2}{\bar{a}^2(\mathbf{r}, t_s)} \frac{\partial^2 p'(\mathbf{r}, t_s, t_f)}{\partial t_f^2} = h(\mathbf{r}, t_s, t_f) \\ + h_c(\mathbf{r}, t_s, t_f) \end{aligned} \quad (17)$$

The explicit expressions of the source term $h(\mathbf{r}, t_s, t_f)$ and $h_c(\mathbf{r}, t_s, t_f)$ are given in [9]. The speed of sound \bar{a} is a local thermodynamic property given by $\bar{a}(\mathbf{r}, t_s) = \sqrt{\gamma \bar{R} \bar{T}(\mathbf{r}, t_s)}$ in a slow-time scale. Boundary conditions on p' are specified in terms of the gradient of p' normal to the boundary surface.

$$\mathbf{n} \cdot \nabla p'(\mathbf{r}, t_s, t_f) = -f(\mathbf{r}, t_s, t_f) - f_c(\mathbf{r}, t_s, t_f) \quad (18)$$

Modal Decomposition of Pressure Oscillations

The pressure oscillations can be modally decomposed in the fast time scale in terms of the mode shape functions $\psi_n(\mathbf{r})$, belonging to a Hilbert space, as:

$$p'(\mathbf{r}, t_s, t_f) = \sum_{n=1}^{\infty} \eta_n(t_s, t_f) \psi_n(\mathbf{r}) \quad (19)$$

subject to the specified boundary conditions of the combustion chamber. In this coordinate frame, $p'(\mathbf{r}, t_s, t_f)$ has a time-dependent component $\eta_n(t_s, t_f)$ along the direction of the n th shape function $\psi_n(\mathbf{r})$ belonging to the set of orthonormal functions $\{\psi_n\}_{n=1,2,\dots}$, which completely spans the space of pressure oscillations. That is, the set $\{\psi_n\}_{n=1,2,\dots}$ satisfies the following conditions:

- Orthonormality: $\langle \psi_n, \psi_m \rangle = \delta_{mn}$ for all integers m and n ;
- Completeness: $\langle \theta, \psi_n \rangle = 0$ for every integer n , implying that $\theta(\mathbf{r}) = 0$ almost everywhere.
- Admissibility: $\{\psi_n\}_{n=1,2,\dots}$ satisfies the specified boundary conditions.

where $\langle \alpha, \beta \rangle \equiv \iiint \alpha(\mathbf{r}) \beta(\mathbf{r}) dV$ defines the inner product in the Hilbert space.

Modal analysis of the acoustic pressure in Eq. 19 is performed with Eqs. 17 and 18 by locally treating the slow-time variables as constants in the fast-time scale:

$$\begin{aligned} \frac{\partial^2 \eta_n(t_s, t_f)}{\partial t_f^2} &= \iiint \frac{\partial^2 p'(\mathbf{r}, t_s, t_f)}{\partial t_f^2} \psi_n(\mathbf{r}) dV \\ &= \sum_{m=1}^{\infty} \eta_m(t_s, t_f) \iiint \bar{a}^2(\mathbf{r}, t_s) \nabla^2 \psi_m(\mathbf{r}) \\ &\quad \psi_n(\mathbf{r}) dV + F_n(t_s, t_f) + U_n(t_s, t_f) \end{aligned} \quad (20)$$

where

$$\begin{aligned} F_n(t_s, t_f) &\equiv - \iiint \bar{a}^2(\mathbf{r}, t_s) h(\mathbf{r}, t_s, t_f) \psi_n(\mathbf{r}) dV \\ &\quad - \iint \bar{a}^2(\mathbf{r}, t_s) f(\mathbf{r}, t_s, t_f) \psi_n(\mathbf{r}) dS \end{aligned}$$

and

$$\begin{aligned} U_n(t_s, t_f) &\equiv - \iiint \bar{a}^2(\mathbf{r}, t_s) h_c(\mathbf{r}, t_s, t_f) \psi_n(\mathbf{r}) dV \\ &\quad - \iint \bar{a}^2(\mathbf{r}, t_s) f_c(\mathbf{r}, t_s, t_f) \psi_n(\mathbf{r}) dS \end{aligned} \quad (21)$$

Space-Time Separation of Mean-Flow Variables

The thermo-acoustic dynamics of the combustion process are parametrically dependent on mean-flow variables. Locally and temporally, smaller mean gas temperature $\bar{T}(\mathbf{r}, t_s)$ implies reduced speed of sound and consequently reduced dominant natural frequencies in the combustion medium, and vice versa. The mean-flow velocity $\bar{\mathbf{v}}_g(\mathbf{r}, t_s)$ represents the coordinate frame in which an acoustic mass element travels. Therefore, $\bar{T}(\mathbf{r}, t_s)$ and $\bar{\mathbf{v}}_g(\mathbf{r}, t_s)$ are used as gain-scheduling parameters for control of mean-flow dependent acoustic dynamics in the fast time scale.

Because $\bar{T}(\mathbf{r}, t_s)$ and $\bar{\mathbf{v}}_g(\mathbf{r}, t_s)$ are continuously varying in both time and space, measurements with finitely many point sensors may lose relevant information. Furthermore, even if distributed sensors are used to measure the spatial distributions of $\bar{T}(\mathbf{r}, t_s)$ and $\bar{\mathbf{v}}_g(\mathbf{r}, t_s)$, the gain-scheduling control law is likely to be excessively time-consuming and hence unsuitable for real-time computation. To synthesize a control law that is executable in real time on an inexpensive computational platform, the mean-flow velocity $\bar{\mathbf{v}}_g(\mathbf{r}, t_s)$ and temperature $\bar{T}(\mathbf{r}, t_s)$ are approximated as the product of a temporal and a spatial variable as:

$$\begin{aligned} \bar{\mathbf{v}}_g(\mathbf{r}, t_s) &\approx \varphi_v(\mathbf{r}) v_t(t_s) \text{ and} \\ \bar{T}(\mathbf{r}, t_s) &\approx \varphi_T(\mathbf{r}) T_t(t_s) \end{aligned} \quad (22)$$

To further enhance the numerical efficiency of the control synthesis computation, the mean flowfield is approximated by a one-dimensional field along the axis of the combustor upon spatial averaging over the cross section. In the sequel, the spatial variable \mathbf{r} is reduced to a scalar variable z in the longitudinal direction, while the temporal variables t_s and t_f remain unaffected.

The one-dimensional mass flow rate through a combustor cross section $A(z)$ is obtained as:

$$\dot{m}(z, t_s) = A(z) \bar{v}_g(z, t_s) \bar{p}(z, t_s) \quad (23)$$

Assuming that the mass flow rate and pressure do not vary significantly along the longitudinal direction of the combustor at every instant t_s in the slow time scale, that is, $\dot{m}(z, t_s) \approx \dot{m}(t_s)$ and $\bar{p}(z, t_s) \approx \bar{p}(t_s)$, it follows from the equation of state that

$$\bar{T}(z, t_s) = \frac{\bar{p}(t_s)}{\bar{R}\dot{m}(t_s)} A(z) \bar{v}_g(z, t_s) \quad (24)$$

For a combustor of uniform cross-section, that is $A(z) = A$ for all z , the one-dimensional flow approximation of Eq. 22 yields:

$$\bar{v}_g(z, t_s) \approx \varphi(z) v_i(t_s) \text{ and } \bar{T}(z, t_s) \approx \varphi(z) T_i(t_s) \quad (25)$$

where $T_i(t_s) = (A\bar{p}(t_s)/\bar{R}\dot{m}(t_s)) v_i(t_s)$ follows from Eq. 24, and the dimensionless spatial weight $\varphi(z) \equiv \varphi_t(z) = \varphi_v(z)$ is normalized over the total length of the combustor, L , that is, $\int_L \varphi(z) dz / L = 1$. The speed of sound is now expressed as:

$$\bar{a}(z, t_s) = a_i(t_s) \sqrt{\varphi(z)} \quad (26)$$

where

$$a_i(t_s) \equiv \sqrt{\bar{\gamma} \bar{R} T_i(t_s)}$$

In the sequel, Eq. 25 is used for control systems analysis and synthesis based on the gain-scheduling variables $v_i(t_s)$ and $T_i(t_s)$ that are generated in real time from the slow-time scale measurements of the variables $\bar{v}_g(z, t_s)$ and $\bar{T}(z, t_s)$. The gain scheduling variables $v_i(t_s)$ and $T_i(t_s)$ together are referred to as the scheduling vector:

$$\vartheta(t_s) \equiv \begin{bmatrix} v_i(t_s) \\ T_i(t_s) \end{bmatrix} \quad (27)$$

Next we proceed to derive a set of ordinary differential equations as an approximation of Eqs. 20 and 21 based on the space-time separation of the mean flowfield in Eq. 25. For a combustion chamber with both ends closed acoustically, a situation encountered in many practical systems, the longitudinal modes of oscillations are obtained as:

$$\psi_n(z) = \cos(n\pi z/L), \quad n = 1, 2, 3, \dots \quad (28)$$

Further, if the speed of sound $\bar{a}(z, t_s)$ does not change significantly along the axis of the combustor, then the orthogonal property of the mode shape functions leads to the following approximate relationship:

$$\int_L \bar{a}^2(z, t_s) \nabla^2 \psi_m(z) \psi_n(z) dz \cong -\omega_n^2 \delta_{mn} \quad (29)$$

for all integers m and n

Substitution of Eqs. 25, 26, and 29 in Eqs. 20 and 21 yields:

$$\frac{d^2 \eta_n}{dt_f^2} + \omega_n^2 (T_i(t_s)) \eta_n = F_n(t_s, t_f) + U_n(t_s, t_f) \quad (30)$$

where

$$F_n(t_s, t_f) = -a_i^2(t_s) \int_L \varphi(z) h(z, t_s, t_f) \psi_n(z) dz$$

and

$$U_n(t_s, t_f) = -a_i^2(t_s) \int_L \varphi(z) h_c(z, t_s, t_f) \psi_n(z) dz$$

where ω_n is the slowly varying frequency of the n th mode, $\omega_n(t_s) = a_i(t_s) k_n$, and k_n is the corresponding wave number. Based on the unforced condition of Eq. 30, the mode shape functions may now be refined from the solution of the following homogeneous equation:

$$\varphi(z) \frac{d^2 \psi_n(z)}{dz^2} + k_n^2 \psi_n(z) = 0 \quad (31)$$

subject to the specified boundary conditions, where the spatially dependent weighting function $\varphi(z)$ exerts a smaller influence in the low-

temperature region and a larger influence in the high-temperature region of the combustion chamber.

Control of Combustion Oscillations

Control actions arising from the spatially distributed combustion of secondary fuel are modeled by an ensemble of M point actuators [2], where each actuator provides acoustic pressure excitation $u_k(\vartheta(t_s); t_f)$, $k = 1, 2, \dots, M$, at predetermined positions z_k , $k = 1, 2, \dots, M$. Accordingly, h_c in Eq. 17 is obtained as a train of temporally varying functions in the following form:

$$h_c(z, t_s, t_f) = \sum_{k=1}^M \delta(z - z_k) u_k(\vartheta(t_s); t_f) \quad (32)$$

The (secondary-fuel) actuator command U_n in Eq. 29, corresponding to the n th mode shape, is obtained as a function of the scheduling vector $\vartheta(t_s)$ in Eq. 27. Fung et al. [2] have presented a detailed derivation of U_n in terms of the heat of combustion per unit fuel mass ΔH_c , the injection rate of secondary fuel \dot{m}_m along with a spatial distribution density b_k , and the time delay τ_k associated with the k th point actuator as follows.

$$U_n = \frac{\bar{R}\Delta H_c}{\bar{C}_v L} \sum_{k=1}^M \psi_n(z_k) u_k(\vartheta(t_s); t_f) \quad (33)$$

where

$$u_k(\vartheta(t_s); t_f) \equiv b_k(\vartheta(t_s)) \frac{\partial \dot{m}_{in} [t_f - \tau_k(\vartheta(t_s))]}{\partial t_f} \quad (34)$$

By considering the first N dominant modes, the open-loop model of the mean-flow dependent acoustic dynamics in the fast-time scale becomes:

$$\begin{aligned} & \frac{\partial^2 \eta_n(t_s, t_f)}{\partial t_f^2} + \omega_n^2(t_s) \eta_n(t_s, t_f) \\ & + \sum_{i=1}^N \left[D_{ni}(\vartheta(t_s)) \frac{\partial \eta_i(t_s, t_f)}{\partial t_f} \right. \\ & \left. + E_{ni}(\vartheta(t_s)) \eta_i(t_s, t_f) \right] \end{aligned}$$

$$\begin{aligned} & \equiv \frac{\bar{R}\Delta H_c}{\bar{C}_v L} \sum_{k=1}^M b_k(\vartheta(t_s)) \psi_n(z_k) \\ & \frac{\partial \dot{m}_{in} [t_f - \tau_k(\vartheta(t_s))]}{\partial t_f} \\ & \text{for } n = 1, 2, 3, \dots, N \end{aligned} \quad (35)$$

State-Space Model of Combustion Dynamics for Control Synthesis

The formulation described in Eq. 35 is considered as a wide-range model of combustion dynamics and provides a framework for accommodating both the global and local behavior in the two time-scale control setting. For both control and estimation, a state-space realization of the combustion dynamics represents a family of ϑ -parameterized models where $\vartheta(t_s)$ is the gain scheduling vector in the slow time scale in Eq. 27. The fast-time-scale state-space model includes uncertainties and effects of mean-flow dependence. The model equations are structurally similar to those derived in Ref. [5]. However, only some, but not all, of the system matrices in the present model are explicit functions of the (slow-time-scale) gain-scheduling vector $\vartheta(t_s)$. For clarity and completeness, these equations are repeated herein.

$$\begin{aligned} \dot{\mathbf{x}}_p(t) &= (A_p(\vartheta) + \Delta_p(\vartheta)) \mathbf{x}_p(t) + G_1(\vartheta) \mathbf{v}(t) \\ & \quad + G_2(\vartheta) \mathbf{d}(t) \end{aligned} \quad (36)$$

$$\mathbf{y}(t) = C \mathbf{x}_p(t) + \boldsymbol{\theta}(t)$$

where the time t represents the fast time t_f . The gain-scheduling vector ϑ consists of mean-flow temperature and velocity as stated in Eq. 27, and is treated as a constant in the fast time scale. The state vector is chosen as $\mathbf{x}_p = [s \dot{s}]^T$ with $\dot{s} = \eta$, and $\eta \equiv [\eta_1 \ \eta_2 \ \dots \ \eta_N]^T$; \mathbf{d} is the plant disturbance; and $\boldsymbol{\theta}$ the sensor noise. For the nominal linear model, the system matrix is given as:

$$A_p \equiv \begin{bmatrix} 0 & I \\ -\Omega(T_f) - E(\vartheta) & -D(\vartheta) \end{bmatrix}$$

$$\text{with } \Omega \equiv \text{diag}(\omega_1^2, \omega_2^2, \dots, \omega_N^2) \quad (37)$$

The fast-time control input vector $\mathbf{v}(t_f)$ associated with a set of point actuators is related to the mass injection rate of the secondary fuel as:

$$\mathbf{v}(\vartheta; t_f) = \begin{bmatrix} b_1(\vartheta)\dot{m}_{in}(t_f - \tau_1(\vartheta) - \delta\tau_1(\vartheta)) \\ b_2(\vartheta)\dot{m}_{in}(t_f - \tau_2(\vartheta) - \delta\tau_2(\vartheta)) \\ \vdots \\ b_M(\vartheta)\dot{m}_{in}(t_f - \tau_M(\vartheta) - \delta\tau_M(\vartheta)) \end{bmatrix} \quad (38)$$

where $\delta\tau_i$ is the modeling error associated with the time delay of the control input. Equation 38 represents the actuator dynamics from the excitation of the point actuator(s) to the actual energy release of control fuel. Unsteady heat release and acoustic pressure provide *effort* and *flow* information in dynamical systems, where their phase difference determines the dissipated or liberated energy.

Because the mean flow varies slowly compared to the effect of the secondary-fuel injection, the transfer function of actuator dynamics is approximated in the s-domain as:

$$A(\vartheta, s) = [b_1(\vartheta)e^{-\tau_1(\vartheta)s} \quad b_2(\vartheta)e^{-\tau_2(\vartheta)s} \quad \dots \quad b_M(\vartheta)e^{-\tau_M(\vartheta)s}]^T \quad (39)$$

An additive operator $\Delta_p(\vartheta; \cdot)$, that is dependent on the mean-flow conditions, represents the effects of parametric inaccuracies and model uncertainties of the plant. The operator Δ_p can be treated as a disturbance to the plant, $\mathbf{w}_s = \Delta_p(\vartheta, \mathbf{x}_p)$, to realize the energy amplification from input to output through this operator. The global behavior of the operator Δ_p is characterized by the L_2 -gain as follows:

$$\|\Delta_p(\vartheta)\|_\infty \leq \delta p(\vartheta) \quad (40)$$

A physical interpretation of Eq. 40 is that individual dynamics of the uncertainty operator Δ_p leads to the following energy amplified relationship from its input \mathbf{x}_p to output \mathbf{w}_s as:

$$\int_0^T \|\mathbf{w}_s\|^2 dt \leq \int_0^T \delta p^2(\vartheta) \|\mathbf{x}_p\|^2 dt \quad \forall T \in [0, \infty) \quad (41)$$

for zero initial conditions.

FORMULATION AND ANALYSIS OF WIDE-RANGE ROBUST CONTROL LAW

This section focuses on robust performance issues of the inner layer within the two-layer

control framework as an extension of the narrow-range control concept presented by Hong et al. [5]. The acoustic dynamics at the inner layer is parametrically dependent on mean-flow dynamics at the outer-layer. For *robustness*, the inner-layer controller is synthesized such that stability is guaranteed over a wide range of (possibly) persistently varying mean-flow variables and the associated modeling uncertainties. For *performance*, the controller should have the capability for rejecting disturbances and meeting the requirements of control energy under both steady-state and transient conditions. The role of the controller design is to simultaneously satisfy these two objectives.

Two-layer Control Structure

In the present two-layer control strategy, the system dynamics is transformed into a combination of a slowly varying trajectory of quasi-steady equilibrium points, defined by the mean-flow dynamics, and the associated perturbations defined in the fast-time scale. While the temporal trajectory of mean-flow variables is tracked for global performance by the slow-time controller, the fast-time controller locally suppresses acoustic motions with its slowly varying parameters being gain-scheduled by the mean-flow temperature and velocity. Figures 1 and 2 show a schematic view of the hierarchical structure of the two-layer control strategy. The inner-layer controller continuously receives gain-scheduled signals from the outer layer to update its parameters, which are related to the temporal equilibrium points defined by the mean-flow temperature and velocity, in response to the change of perturbation dynamics at quasi-steady equilibrium points. It also simultaneously processes the fast-time-scale signals of pressure oscillations. The modulated signals then manipulate the actuators of the combustion chamber to locally suppress perturbations along the temporal trajectory of the mean-flow variables for wide-range control of combustion dynamics.

Analysis of Robust Control Law

To design the robust inner-layer controller, a family of gain-scheduled (i.e., ϑ -parameterized) generalized plants is first constructed following

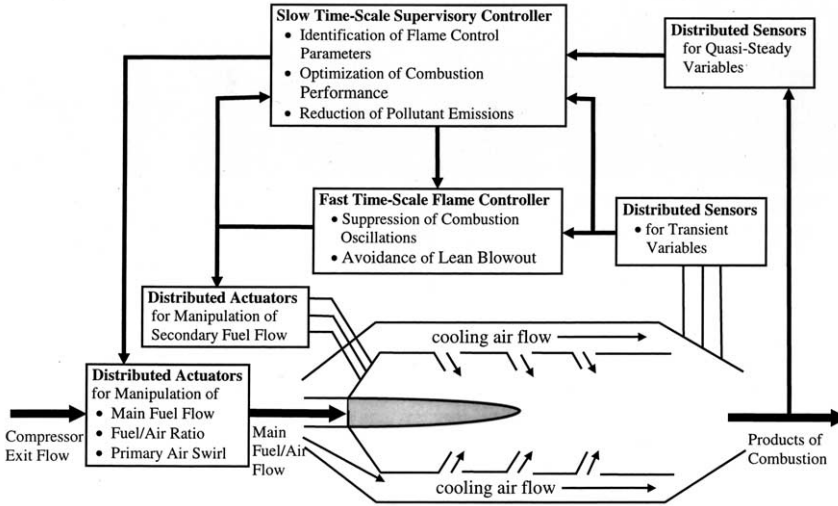


Fig. 1. Two-Layer Control System for Modulating Combustion Dynamics.

the block diagram in Fig. 3. It includes the ϑ -parameterized nominal plant, actuator dynamics, modeling uncertainties, and performance requirements for synthesis of a wide-range robust control law. The feedback controller $K(s; \bar{v})$ is derived as a function of the gain-scheduling vector ϑ for controller adaptation under slowly varying operating conditions. Figure 3 shows the internal structure of the ϑ -parameterized generalized plants. The metric of L_2 -gain facilitates transformation of the coupled performance-stability robustness analysis problem into a stability robustness problem [10]. To incorporate the disturbance rejection capabilities for robust performance, the control objective is related to the metric of L_2 gain, indicating energy amplification from the generic disturbance w to the objective variable z . The generic disturbances w consist of disturbances

induced by plant uncertainties w_s and by ϑ -parameterized modeling errors of the time delay function w_τ , weighted plant disturbances w_d , and weighted sensor noise w_θ . The objective variable z consists of stability variables associated with plant uncertainty z_s and time-delay errors z_τ , and performance variables associated with the acoustic pressure response z_p and the secondary-fuel injection z_u .

The subsystems in the generalized plant family are the nominal plant dynamics specified in the ϑ -parameterized state-space realization, (A_p, G_1, G_2, C) , shaping filters associated with the plant disturbances W_d , sensor noise W_θ , performance weighting functions associated with pressure response and secondary-fuel in-

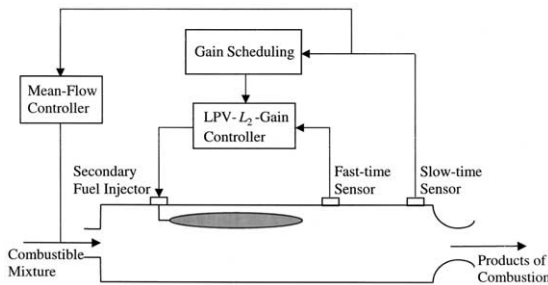


Fig. 2. Two-Layer Robust Control System for Modulating Combustion Dynamics.

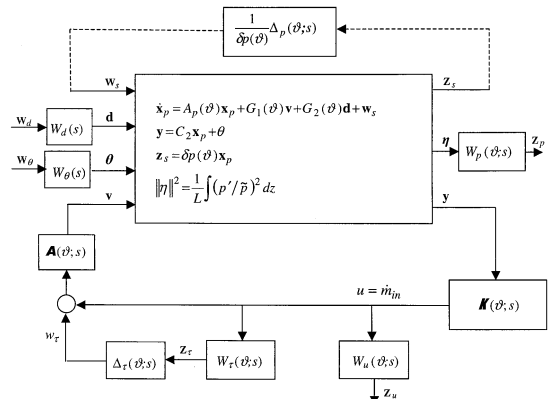


Fig. 3. Generalized Plant of Combustion Dynamics.

jection, W_p and W_u , respectively, and the stability weighting function associated with time-delay errors, W_τ . Note that the plant uncertainty Δ_p and phase uncertainty induced by time-delay errors Δ_τ are not included, because modeling uncertainties are represented as uncertainty-induced disturbances, w_s and w_τ . Two shaping filters W_d and W_θ are incorporated to characterize the main frequency components of the plant disturbances and sensor noises. The performance weighting functions W_p and W_u are specified for the desired frequency responses of acoustic motions and secondary-fuel injection, respectively, providing the trade-off between (high-frequency) transient and (low-frequency) quasi-steady-state responses. Those subsystems are derived as analytic functions of the gain-scheduling vector ϑ to serve as the database of the LPV controller synthesis.

In modeling the secondary-fuel distribution, the parametric error of time delay $\delta\tau(\vartheta)$ causes ϑ -parameterized phase uncertainty of the closed loop. The corresponding transfer function $e^{-\delta\tau(\vartheta)s}$ is represented as a member of the following set:

$$\{(1 + \Delta_\tau(\vartheta; j\omega) W_\tau(\vartheta; j\omega) \quad \forall \omega \quad \forall \vartheta: \|\Delta_\tau(\vartheta; j\omega)\| \leq 1\} \quad (42)$$

where $\Delta_\tau(\vartheta; j\omega)$ accounts for the phase uncertainty and acts as the magnitude scaling for each component of ϑ . The stability weighting function $W_\tau(\vartheta; j\omega)$ specifies allowable joint phase-magnitude margins in the closed-loop system and serves as a metric of robustness. Equation 42 is equivalent to:

$$|e^{-\delta\tau(\vartheta)j\omega} - 1| \leq |W_\tau(\vartheta; j\omega)| \quad \forall \omega \quad \forall \vartheta \quad (43)$$

where

$$\delta\tau(\vartheta) \equiv \max_k |\tau_k(\vartheta)| \quad \forall \vartheta.$$

For the second source of modeling uncertainty, the plant uncertainty $\Delta_p(\vartheta; s)$ acts as an internal feedback to the nominal dynamics. It accounts for modeling inaccuracies of intrinsic coupling between flow dynamics and combustion responses. The bound of $\Delta_p(\vartheta; s)$ is specified by its L_2 gain as $\|\Delta_p(\vartheta; s)\|_\infty < \delta p(\vartheta)$. Based on the small gain theorem [10], a sufficient condition for robust stability of the closed-loop system for the zero-state initial conditions with z_s equal to $\delta p(\vartheta)\mathbf{x}_p$ is:

$$\int_0^T (\|z_s\|^2 + \|z_\tau\|^2) dt \leq \int_0^T (\|w_s\|^2 + \|w_\tau\|^2) dt \quad \forall T \in [0, \infty) \quad (44)$$

The inequality in Eq. 44 implies that the robust controller can stabilize all perturbed plants within the ϑ -parameterized uncertainty bounds characterized by $\delta p(\vartheta)$ and $\delta\tau(\vartheta)$ without specifying any performance requirements that provide the trade-off among the control versus acoustic energy, transient versus steady-state response, and stability robustness and performance. The performance weights within the system bandwidth are included in the generalized plants for regulation of the secondary-fuel injection and acoustic dynamics. Shaping filters are used to penalize the dominant frequency components of plant disturbances and sensor noises for effective rejection. The ability to suppress flow oscillations is quantified by a positive (dimensionless) quadratic energy-like function:

$$H(t_s, t_p) = \frac{1}{L} \int |p'(z, t_s, t_p) / \bar{p}(z, t_s)|^2 dz \quad (45)$$

Orthonormality of the acoustic mode shape functions simplifies Eq. 45 as:

$$H = \langle \sum \varphi_n \eta_n, \sum \varphi_m \eta_m \rangle = \sum \eta_n^2 = \|\eta\|^2 \quad (46)$$

The combustion chamber becomes free of pressure oscillations if the energy function H approaches zero.

To achieve small limit-cycle amplitudes and short settling time of pressure oscillations, a new performance variable \mathbf{z}_p is introduced as:

$$\hat{\mathbf{z}}_p(s) = W_p(\vartheta; s) \hat{\boldsymbol{\eta}}(s) \quad (47)$$

where the Laplace transform of a time-dependent quantity is denoted by the hat “ \wedge ” symbol; and the weighting function $W_p(\vartheta; s)$ is defined as:

$$W_p = \begin{bmatrix} W_{p1} & 0 & \cdots & 0 \\ 0 & W_{p2} & \ddots & \vdots \\ \vdots & \ddots & \ddots & 0 \\ 0 & \cdots & 0 & W_{pN} \end{bmatrix} \quad (48)$$

A procedure for selecting the performance weighting matrix $W_p(\vartheta; s)$ of pressure oscillations

tions is now outlined. The Bode plot of $W_{pi}(\vartheta; s)$, $i = 1, 2, \dots, N$ resembles that of an integration operator within the bandwidth around each natural frequency $\omega_i(\vartheta)$ over the range of the gain-scheduling variable ϑ . The shape of each $W_{pi}(\vartheta; s)$ outside the respective bandwidth is assigned to be flat. The amplitude of each $W_{pi}(\vartheta; s)$ represents the extent of overshoot of the amplitude of its mode shape for the trade-off between transient and steady-state responses, in the sense that a high overshoot usually leads to a short settling time. Thus, the resulting performance variable z_p yields small steady-state amplitude and short settling time of pressure fluctuations. Note that the bandwidth of $W_{pi}(s)$ could be altered by mean-flow-dependent modeling uncertainties. The nominal bandwidth corresponds to the natural frequency of acoustic oscillations. To determine the possible bandwidth range for all perturbed plants, natural frequencies within the uncertainty bound of ϑ need to be calculated.

The other performance requirement involves secondary-fuel injection. The frequency response of the mass flow rate of secondary fuel has limited bandwidth and overshoot amplitude due to the inertial effects of the fuel flow. To this end, a performance weight $W_u(\vartheta; s)$ is incorporated into the generalized plant model, and a new performance variable z_u is defined as:

$$\hat{z}_u(s) = W_u(\vartheta; s)\hat{u}(s) \tag{49}$$

where $\hat{u}(s)$ and $\hat{z}_u(s)$ are the Laplace transforms of $\dot{m}_{in}(t)$ and $z_u(t)$, respectively. The ϑ -parameterized performance weighting $W_u(\vartheta; s)$ is chosen via the following procedure. The Bode plot of $W_u(\vartheta; s)$ resembles that of a derivative operator within the frequency range of interest. A small z_u implies that the high-frequency component of the secondary fuel flow rate \dot{m}_{in} has been filtered out. At each ϑ , the shape of W_u outside the bandwidth is assigned to be flat. The bandwidth range is altered by uncertainties in the (mean-flow-dependent) scheduling vector ϑ .

The nominal performance is specified by the relationship between exogenous inputs, plant disturbance d and sensor noise θ , and performance variables, z_p and z_u . A shaping filter W_d is included in the generalized plant such that the

resulting robust controller focuses on rejecting the dominant frequency components of plant disturbances. Therefore, the weighted plant disturbance w_d is used for performance specifications, instead of the disturbance d itself, where

$$\hat{w}_d(s) = W_d(s)\hat{d}(s) \tag{50}$$

Similar conditions are introduced for the sensor noise θ as:

$$\hat{w}_\theta(s) = W_\theta(s)\hat{\theta}(s) \tag{51}$$

where \hat{w}_θ is the weighted sensor noise and W_θ the shaping filter.

A linear parameter varying (LPV) robust controller was designed such that the plant disturbance d and sensor noise θ have insignificant effects on the acoustic motions and control actions from the energy perspectives. The nominal performance is specified by:

$$\int_0^T \|q(\vartheta)z_p(t)\|^2 + \|z_u(t)\|^2 dt \leq \int_0^T (\|w_d(t)\|^2 + \|w_\theta(t)\|^2) dt \quad \forall T \in [0, \infty) \tag{52}$$

where q is a ϑ -parameterized positive scalar, representing the weighting factor of acoustic motion. If q is set larger, the response of acoustic motions becomes more emphasized than that of control actions, and vice versa. Furthermore, increasing q implies a better ability to reject exogenous inputs.

Based on Eq. 44 and Eq. 52, a sufficient condition for robust performance (i.e., a combination of robust stability and nominal performance) of the control system is:

$$\int_0^T \|z\|^2 dt \leq \int_0^T \|w\|^2 dt \quad \forall T \in [0, \infty) \tag{53}$$

$$\forall w \in L_2[0, T];$$

$$\text{with } z = \begin{bmatrix} z_s \\ qz_p \\ z_u \\ z_\tau \end{bmatrix}; w = \begin{bmatrix} w_s \\ w_d \\ w_\theta \\ w_\tau \end{bmatrix}$$

If Eq. 53 holds, then the controller internally stabilizes the closed loop for all perturbed plants with desired performance, subject to an uncertainty bound.

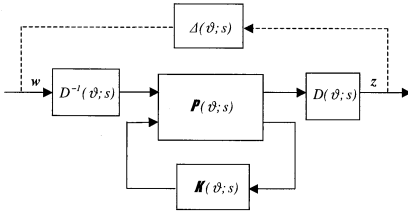


Fig. 4. Compensated Generalized Plant of Combustion Dynamics.

Following the internal structure in Fig. 3, a family $P(\vartheta; s)$ of generalized plant models is constructed, similar to what was established for narrow-range control [5]. The state-space realization of a generalized plant model has the following structure:

$$\begin{aligned} \dot{\mathbf{x}} &= A(\vartheta)\mathbf{x} + B_1(\vartheta)\mathbf{w} + B_2(\vartheta)u \\ z &= C_1(\vartheta)\mathbf{x} + D_{12}(\vartheta)u \\ y &= C_2(\vartheta)\mathbf{x} + D_{21}(\vartheta)\mathbf{w} \end{aligned} \quad (54)$$

Note that Eq. 53 is conservative because it ignores the structure of the uncertainly robust performance operator $\Delta(\vartheta; s)$, which consists of model uncertainties and performance-induced uncertainties. The generalized plant family $P(\vartheta; s)$ in Eq. 54 can be compensated to make the requirements of robust performance specified in Eq. 53 less conservative. Figure 4 shows that the generalized plant family is compensated by two ϑ -parameterized compensators, $D^{-1}(\vartheta; s)$ and $D(\vartheta; s)$. The resultant system represents the structure Δ without altering the uncertainty size and performance requirements. This is achieved by choosing the D -compensator as:

$$D(\vartheta; s)\Delta(\vartheta; s) = \Delta(\vartheta; s)D(\vartheta; s) \quad \forall \vartheta \quad (55)$$

This compensation approach, known as the D-K iteration [10], can be repeated to arrive at the final result.

SYNTHESIS OF WIDE-RANGE ROBUST CONTROL LAW

The inner-layer control law is synthesized using the concept of linear parameter varying (LPV)- L_2 -gain methodology. The objective is to reject the effects of chamber disturbances and mean-

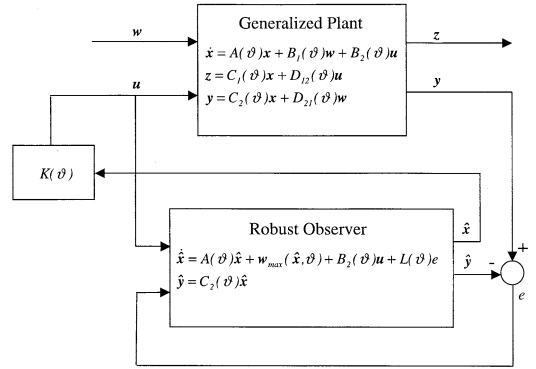


Fig. 5. Synthesis of Robust LPV Control System.

flow-dependent model uncertainties while optimizing the specified performance. The LPV- L_2 -gain controller has a H_∞ -structure and is derived as a gain-scheduling process accommodating continuous variations of the mean-flow conditions. The major challenge is to synthesize a family of ϑ -parameterized control laws that guarantee robust performance under continuously varying mean-flow conditions over a wide operating range.

The LPV L_2 -gain controller consists of two main components. The first component is a ϑ -parameterized observer that dynamically estimates the states of the ϑ -parameterized generalized plant models described by Eq. 54. The estimator structure is not formulated as an exact plant state observer due to the presence of a calibration term $w_{cal}(\vartheta)$ in the observer state equation that protects the control system from being excessively sensitive to exogenous inputs and modeling uncertainties. The second component is a state-feedback control gain matrix, which determines the control action based on the estimated state \hat{x} as seen in the controller configuration of Fig. 5.

The remaining task in the control synthesis procedure is to determine the ϑ -parameterized observer matrix, controller matrix, and the calibration term such that the sufficient condition for robust performance in Eq. 53 holds. Usage of parameter-dependent Lyapunov functions in the controller synthesis leads to differential matrix inequalities that need to be solved as simultaneous inequalities. Mathematical details are reported by Hong et al. [6] and Hong [11].

TABLE 2

Parameters of Generic Combustion Chamber	
Average mean speed of sound	795.8 m/s
Average mean temperature, T_0	1415 K
Average mean pressure, p_0	0.5 MPa
Combustor length, L	1.0 m
Combustor diameter, d_c	0.6 m
Specific heat ratio, $\bar{\gamma}$	1.2
Gas constant, \bar{R}	373 J/(kg · K)
Constant volume specific heat, \bar{C}_v	1500 J/(kg · K)
Heat of combustion of control fuel, ΔH_c	5×10^6 J/kg
Average fundamental frequency, $\omega_0 \equiv \pi a_0/L$	1000 rad/s
Average mean velocity, v_0	300 m/s
Average mixture density, $\bar{\rho}$	0.947 kg/m ³

TABLE 3

Dimensionless Quantities	
Dimensionless time, t'	$\omega_0 t$
Dimensionless frequency, ω'	ω/ω_0
Dimensionless mass injected rate of control fuel, u'	$\frac{-\bar{R}\Delta H_c}{\omega_0^2 \bar{C}_v p_0} u$
Dimensionless damping ratio, D'_{ni}	D_{ni}/ω_0
Dimensionless frequency shifting, E'_{ni}	E_{ni}/ω_0^2
Dimensionless gain-scheduling mean velocity, ρ_v	v_t / v_0
Dimensionless gain-scheduling mean temperature, ρ_T	T_t/T_0
Dimensionless ρ_v variation rate, $\dot{\rho}_v$	$d\rho_v/dt'$
Dimensionless ρ_T variation rate, $\dot{\rho}_T$	$d\rho_T/dt'$

SIMULATION RESULTS AND DISCUSSION

A series of parametric studies for a generic combustor have been conducted to validate the wide-range robust control methodology. The objective is to investigate the relationships among system performance, stability robustness, and plant operation based on the transient response of the acoustic field under different operation scenarios. The effects of the uncertainty bounds of system dynamics, the trade off between flow oscillations and control actions, and the allowable variation rates of mean-flow parameters are investigated and quantified.

Table 2 lists the parameters of a generic combustor that represents typical scenarios encountered in practical combustion chambers. The linear parameters D_{ni} and E_{ni} in the nominal model, Eq. 35, as well as the spatial distribution b_n and time delay τ_n of the combustion source, are taken from [2]. The dimensionless quantities that are required for investigating longitudinal acoustic oscillations based on various control strategies are given in Table 3. The simulation parameters are summarized in Table 4.

The gain scheduling vector ϑ in Eq. 27 is generated in real time from the measurements of mean flow variables in the slow-time scale. Two bandwidth-limited performance weighting functions W_p and W_u have been fitted as continuous functions of the scheduling variables at selected modal frequencies $\omega_1, \dots, \omega_N$. The shaping filters W_d and W_θ are taken as unity as the chamber disturbances and sensor noise are assumed to be white Gaussian. System robust-

ness and performance are represented by the bound $\delta p(\vartheta)$ of plant modeling uncertainties and the weighting factor of pressure response $q(\vartheta)$, respectively. Plant operation is characterized by the bounds of absolute values of the normalized rates of the scheduling variables $|\dot{\rho}_T| \equiv |\dot{T}_t/T_t|$ and $|\dot{\rho}_v| \equiv |\dot{v}_t/v_t|$. Increasing $|\dot{\rho}_T|$ and $|\dot{\rho}_v|$ implies that the scheduling variables can be varied faster with guaranteed robust performance. On the other hand, increasing the performance parameter q implies a more stringent requirement of system performance in terms of the transient oscillation of each acoustic mode and the ability to reject chamber acoustic and thermal noises. Extensive simulation experiments have been conducted to realize the trade-off relationship among system robustness, performance, and operation of the control system. The time history and frequency spectrum of acoustic pressure transients are generated based on simulation experiments at several points of the two slowly varying trajectories of mean-flow temperature and velocity.

The dimensionless bounds of the variation

TABLE 4

Parameters Used in Simulation and Modeling	
Maximum time delay error	$\delta\tau = 3/\omega_0$
Plant uncertainty bound	$\delta p = 0.03$
Weighting factor	$q = 0.1$
White plant-disturbance intensity	$0.1 \times \frac{\omega_0^2 \bar{C}_v p_0}{\bar{R}\Delta H_c}$
White sensor-noise intensity	$0.1 \times \frac{\omega_0^2 \bar{C}_v p_0}{\bar{R}\Delta H_c}$

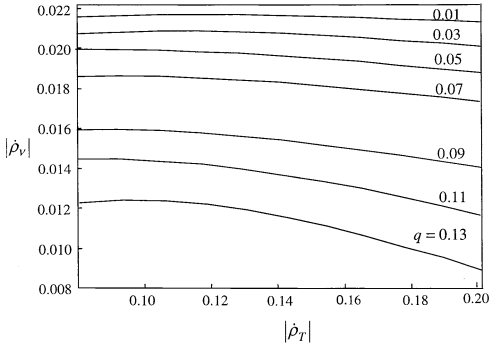


Fig. 6. Trade-off between Performance and Plant Operation.

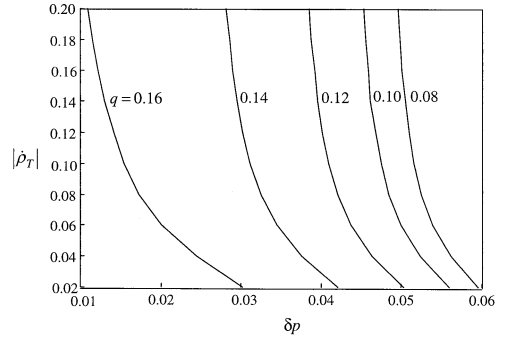


Fig. 7. Trade-off between Robustness and Performance.

rates $|\dot{\rho}_T|$ and $|\dot{\rho}_v|$ jointly define the allowable varying rate of plant operation from the perspective of performance. Figure 6 shows the trade-off between system performance and plant operation. For the plant uncertainty bound set at $\delta\rho = 0.03$, the family of curves in Fig. 6 serve as a constraint under which the LPV robust controller guarantees system stability and performance in the operating range of $\rho_T \in [0.6, 1.4]$ and $\rho_v \in [0.5, 1.5]$. The triple $(|\dot{\rho}_T|, |\dot{\rho}_v|, q)$ defines the design point that is evaluated during the modeling phase before the controller design. For example, with the maximum values of the mean temperature and velocity $|\dot{\rho}_T|$ and $|\dot{\rho}_v|$ being 0.1 and 0.016, respectively, the weighting factor of the system performance q should be less than or equal to 0.09 to guarantee robust performance. This is a conservative design and, in the simulation stage, much larger q may be allowed. A larger q leads to a larger risk, because it implies a larger probability that the combustion system may enter into a (potentially) unstable region beyond what is specified by the plant uncertainty model. The insufficient information on uncertainty dynamics, despite the size specified by the induced L_2 -norm, prevents precise quantification of the region of risk. Figure 6 qualitatively reveals the sensitivity of each design point. Robust performance of the closed-loop system is sensitive to the mean-velocity variation rate $\dot{\rho}_v$ because the L_2 -gain control tends to maximize the entropy of the closed-loop system. The effects of mean-velocity rate $\dot{\rho}_v$ on the dissipation or driving of acoustic dynamics represent the varying conditions of the irreversible process in the acoustic

field. Because the entropy-oriented scheme is sensitive to the controlled irreversible process, the L_2 -gain control system of acoustic dynamics is sensitive to mean-velocity variations. Figure 6 also suggests that the robust performance of the closed loop is relatively insensitive to the mean-temperature variation rate $\dot{\rho}_T$ because the mean temperature determines the natural frequencies of the acoustic field. This phenomenon also leads to the fact that the bandwidth of the open-loop system is almost the same as that of the closed-loop system. In other words, the feedback control does not change the natural frequencies of the system. Therefore, model reduction originally performed for the open-loop plant remains valid for the closed-loop system. Consequently, for large natural frequencies, the control actions would require fast actuators.

Figure 7 shows that the robust performance of the closed-loop system is not very sensitive to mean temperature variation rate for $|\dot{\rho}_v|$ being set to 0.01. The results indicate that robustness of the closed-loop system becomes sensitive to

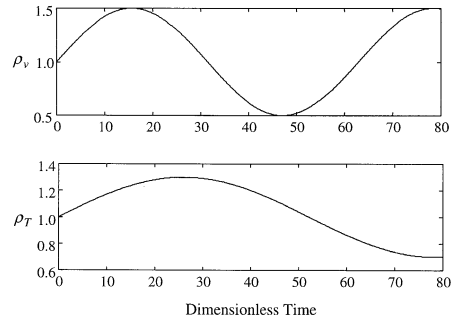


Fig. 8. Time History of Mean Velocity and Temperature.

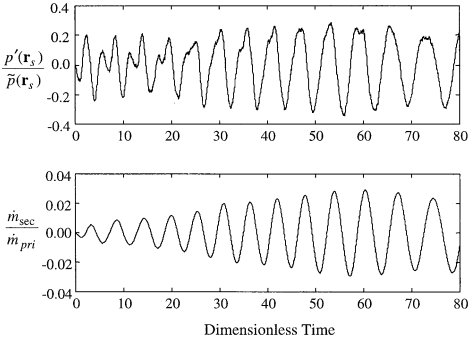


Fig. 9. System Response under H_∞ Control.

mean-velocity variation rate only in the region of high performance. Figure 7 can be also used to realize a trade-off between robustness δp and performance q . In the low-performance region, the trade-off between robustness and performance is almost linear. That is, the increment of δp is approximately proportional to the decrement of q .

In the simulation of the closed-loop system for a wide range of mean-flow conditions, the plant uncertainty bound is set to be $\delta p = 0.03$, time delay uncertainty bound $\delta \tau = 3/\omega_0$, plant disturbance intensity $0.1 \times \omega_0^2 \bar{C}_v p_0 / \bar{R} \Delta H_c$, and sensor noise intensity $0.1 \times \omega_0 \bar{C}_v p_0 / \bar{R} \Delta H_c$. The temporal trajectories of the mean velocity and temperature are shown in Fig. 8. Three different controllers (i.e., single H_∞ control, gain-scheduled control, and LPV L_2 -gain control) are considered as follows.

Figure 9 shows the system response using a single H_∞ controller for the entire range of $\rho_T \in [0.6, 1.4]$ and $\rho_v \in [0.5, 1.4]$, where the system response exhibits instability and hence the per-

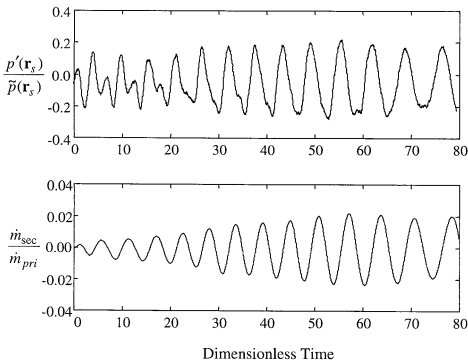


Fig. 10. System Response under Gain-Scheduled Control.

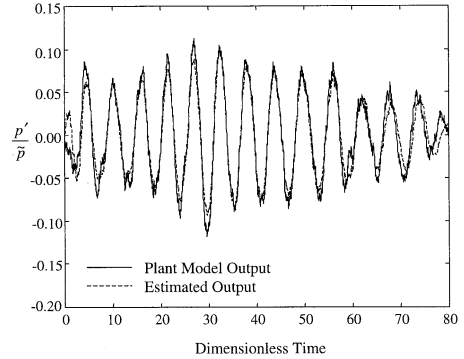


Fig. 11. Time History of First Mode of Pressure Oscillation under LPV- L_2 Gain Control.

formance is obviously unacceptable. Note that H_∞ control may be suitable for narrow-range operation as discussed in the previous work [5], but not for wide-range operation here. Figure 10 shows the system performance of the gain-scheduled controller, which is synthesized without considering the variations in the mean-flow variables \bar{T} and \bar{v}_g . The results show that the control system is also unstable. This establishes the necessity of LPV robust control.

Figures 11–14 show the responses of the first four modes of acoustic oscillation in the chamber under LPV robust control. The total acoustic oscillations are significantly improved since the controller exhibits the ability to reject exogenous inputs on the first two modes without degrading the responses of high-frequency modes. This suggests that model reduction has not caused any significant loss of robustness under the LPV control for wide-range operation. Therefore, the usage of the LPV robust

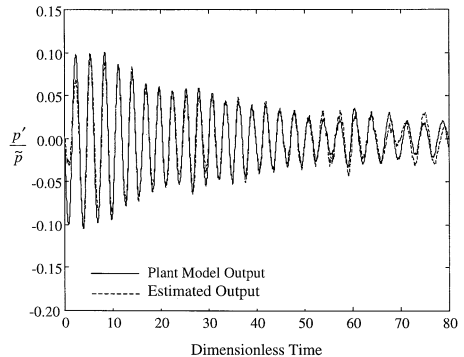


Fig. 12. Time History of Second Mode of Pressure Oscillation under LPV- L_2 Gain Control.

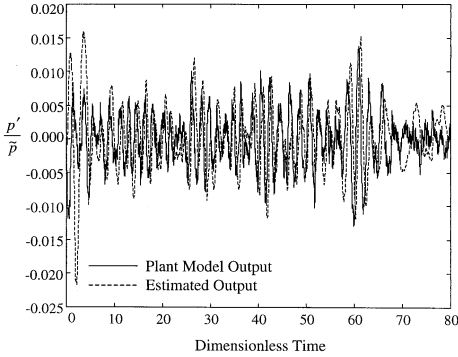


Fig. 13. Time History of Third Mode of Pressure Oscillation under LPV- L_2 Gain Control.

control may not require a meticulous consideration of high-frequency excitations provided that the scheduling variables are appropriately rate-bounded. It is also shown that the closed loop system is asymptotically stable in the absence of exogenous inputs.

The embedded observer located in the LPV robust controller is capable of estimating the internal states of acoustic dynamics under a wide range of continuously varying mean-flow conditions, as evident in Figs. 11–14. The embedded observer provides an estimation of acoustic vibration of each mode. The transient and quasi-steady-state errors, because of modeling uncertainties and exogenous inputs, are shown to be small. The calibration terms in the embedded observer are able to keep the system away from the high-risk region, and yet they are small enough not to significantly change the estimated states. In the absence of modeling uncertainties, the performance of the observer

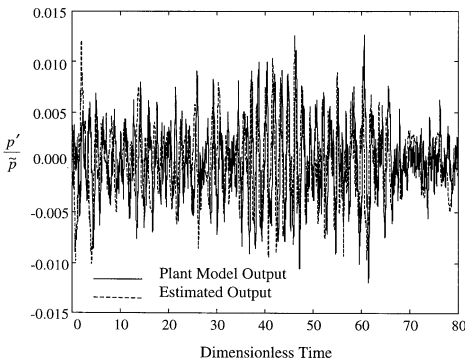


Fig. 14. Time History of Fourth Mode of Pressure Oscillation under LPV- L_2 Gain Control.

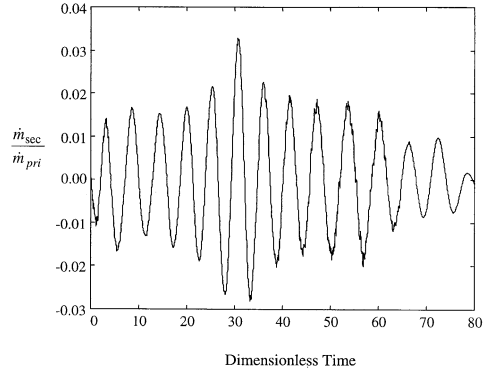


Fig. 15. Secondary Fuel Injection Rate under LPV L_2 - Gain Control.

embedded in the L_2 -gain controller approaches that of the minimum variance state estimator.

Figure 15 shows the secondary-fuel injection in the LPV robust control system. The fast-time modulation is less than 4% of the primary fuel flow rate, whereas the amplitude of acoustic pressure oscillations exceeds 10% of the mean pressure. Figure 16 shows the frequency spectrum of the normalized pressure perturbations before and after the controller is activated.

SUMMARY AND CONCLUSIONS

To synthesize a robust control law for wide-range operations, a two-time-scale formulation of combustion dynamics has been developed. The model equations are formulated by decomposition of the conservation laws and thermodynamic state relations based on the slowly varying mean flow field and fast varying oscilla-

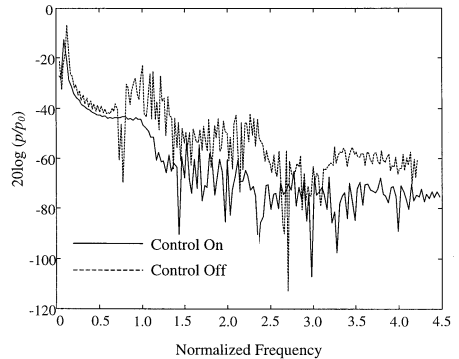


Fig. 16. Frequency Spectrum of Pressure with and without LPV L_2 - Gain Control.

tion flow field. Control actions on the fast time scale are provided by secondary fuel injection. The structure of the wide-range control system follows a two-layered hierarchy. In the outer layer, mean-flow dynamics of the combustion process is controlled in the slow time scale by manipulating the primary-fuel flow, while the fast-time-scale acoustic controller in the inner layer is parametrically gain-scheduled by the mean-flow temperature and velocity from the outer layer.

In the fast-time scale inner layer, a robust control law is formulated based on the concept of LPV L_2 -gain in the setting of differential game theory. The control law has an embedded observer that dynamically estimates the plant states. Time derivatives of the gain-scheduling variables need not be computed or estimated to realize the interactions between the inner-layer and outer-layer segments of the control system.

For both narrow and wide-range conditions of the mean-flow variables, the control law is designed in terms of robustness, performance, and parameter variation rate. Procedures for selection of mean-flow-dependent and frequency-dependent weighting functions have been proposed in this paper. The physics of the thermo-acoustic phenomena have a significant bearing upon the selection of these performance weights. By appropriate selection of these performance weights, a robust control law can be synthesized in a few iterations. In addition, a numerical tool for synthesis of the LPV robust control law is established based on the concept of finite-element analysis. Parametric studies and simulation experiments have been performed to evaluate the robust control system in terms of the trade-off among: (1) control injection requirement and pressure oscillations; (2) transient and steady response; and (3) stability robustness and performance.

Results reported in this paper lead to a design methodology for wide-range robust control of pressure oscillations in a generic combustor. The findings could be applied to a multitude of other combustion processes. Although the simulated results clearly indicate efficacy of the robust controller design methodology, several issues concerning implementation of robust control laws need to be addressed before application to operating combustors.

The research work reported in this paper was supported in part by the Office of Naval Research under Grant No. N00014-96-1-0405, and in part by The Pennsylvania State University.

REFERENCES

1. Yang, V., Santavicca, D. A., and Ray, A., *Proceedings of Twelfth Propulsion Meeting*, U.S. Office of Naval Research, Arlington, VA, 1999, pp. 61–66.
2. Fung, Y. T., Yang, V., and Sinha, A., *Comb. Sci. Technol.* 78:217–245 (1991).
3. Yang, V., Sinha, A., and Fung, Y. T., *J. Propulsion and Power* 8:66–73 (1992).
4. Fung, Y. T. and Yang, V., *J. Propulsion and Power* 8:1282–1289 (1992).
5. Hong, B. S., Yang, V. and Ray, A., *Comb. Flame* 120:91–106 (2000).
6. Hong, B. S., Ray, A. and Yang, V., Parameter-Dependent L_2 -Gain Control Synthesis, *American Control Conference*, Chicago, IL, June 2000, pp. 3697–3701.
7. Wu, F., Yang, X. H., Packard, A. and Becker, G., *Intl. J. Robust and Nonlinear Control*, 6:983–998 (1996).
8. Gahinet, P. and Apkarian, P., *Intl. J. Robust and Nonlinear Control*, 4:421–448 (1995).
9. Fung, Y. T., *Active Control of Linear and Nonlinear Pressure Oscillations in Combustion Chambers*, Ph.D. Thesis, The Pennsylvania State University, 1991.
10. Zhou, K., Doyle, J. C., and Glover, K., *Robust and Optimal Control*, Prentice-Hall, New Jersey, 1996.
11. Hong, B. S., *Robust Control of Combustion Instabilities*, Ph.D. Thesis. The Pennsylvania State University, 1999.

Received 8 May 2001; revised 10 October 2001; accepted 2 November 2001